Journal of Earth Sciences and Geotechnical Engineering, Vol. 15, No. 1, 2025, 1-37
ISSN: 1792-9040 (print version), 1792-9660 (online)
https://doi.org/10.47260/jesge/1511
Scientific Press International Limited

Numerical Analysis of the Large-scale Dynamic Tests of Rock Support at Kiirunavaara mine

Shirzadegan Shahin[1], Nordlund Erling[2], Zhang Ping[2], Yi Changping[2] and Warema Senzia[2]

Abstract

The numerical analysis of four dynamic large-scale field tests conducted at LKAB Kiirunavaara mine are presented in this paper. The aim was to numerically study the behavior and response of the burden and the tested walls in field Tests 1, 2, 4 and 5. For this purpose, two numerical methods were combined, i.e. the finite element code LS-DYNA and the distinct element code UDEC. The LS-DYNA was used to calculate the blast load, and the UDEC was used to propagate the calculated load in the model where the geological conditions of the test site and the installed rock support in the field tests were modelled. The model was calibrated by comparing the velocity and displacement calculated on the surface of the opening, and the zones yielded in tension were used to study the failure mechanism developed in the burden. The numerical models were able to mimic the behavior of the jointed rock mass and the rock support fairly well. It is concluded that the number of major joint sets was the main reason to the difference between the failure development in Tests 1 and 2 and Tests 4 and 5. The numerical analysis of Tests 1 and 2 confirmed that the gas pressure in the vicinity of the test wall in those tests was minimum. In Tests 4 and 5, it was observed that, the generated fractures in the burden combined with the natural joint condition of the burden, increased the possibility for blocks to rotate and move within the burden. The complete burden damage in Tests 4 and 5 was concluded to be the be due to the ejection of rock blocks in the vicinity of the test wall upon the arrival of stress wave, and ejection of the remaining portion of the rock blocks in the burden by the gas expansion.

Keywords: UDEC, LS-DYNA, Numerical analysis, Large-scale tests, Rock support.

[1] Ramboll Sweden AB, Rock Engineering Division.
[2] Luleå University of Technology.

Article Info: Received: November 7, 2024. Revised: November 27, 2024.
Published online: January 9, 2025.

1. Introduction

A series of large-scale dynamic tests were conducted in the Kiirunavaara underground mine (owned and operated by LKAB) with the main objectives to develop a methodology for in-situ testing of rock support under dynamic conditions, and to investigate the response of the openings and the installed support system to strong dynamic loads. In these tests, blasting was used to generate the seismic load. Large-scale dynamic tests of rock support have previously been conducted in different mines since 1969 (Ortlepp, 1969; Ortlepp, 1992; Tannant et al., 1994; Tannant et al., 1995; Ansell, 1999; Hagan et al., 2001; Espley et al., 2002; Archibald et al., 2003; Ansell, 2004; Andrieux et al., 2005; Heal et al., 2005; Heal and Potvin, 2007; Heal, 2010). A review of the previously conducted tests was presented in Shirzadegan et al. (2016b).

The tests conducted in the Kiirunavaara mine (Tests 1 to 7) are divided into two design categories, (i) the tests with a shallow burden of 2.8 – 3.9 m, including Tests 1, 2, 4 and 5 reported by Shirzadegan et al. (2016b), and (ii) the tests with a deep burden of 8.1 – 8.9 m, including Tests 6 and 7 in Shirzadegan et al. (2016a). The results obtained from Tests 1, 2, 4 and 5 showed that detailed numerical analyses were required to answer the questions that had been formulated based on the results of tests. The main questions were (a) why was the level of damage observed on the tested walls minimal despite the high PPVs measured on the surface of the test wall in Tests 1 and 2? (b) what was the reason for complete destruction of the burden in Tests 4 and 5 even though the burden was similar to that in Tests 1 and 2?

This paper focuses on developing numerical models of Tests 1, 2, 4 and 5 by considering the possible jointing conditions of the burden and their effect on the velocity and displacement of the test wall surface, and the type of damage induced to the burden and test wall. Furthermore, the performance of the installed rock support in Tests 1, 2, 4 and 5 are investigated numerically and its role in Tests 1 and 2, with minimal damage, and in Tests 4 and 5, with complete destruction of the test burden is discussed.

The numerical methods used to analyze Tests 1, 2, 4 and 5 consisted of a combination of the finite element code, LS-DYNA and the discrete element code UDEC. The LS-DYNA code was used to calculate the diameter of the crushed zone boundary (CZB) created around the blasthole and the blast load (in terms of velocity versus time) at the CZB. The CZB and the calculated velocity of that boundary was used as input in the UDEC model. The method has previously been used by Chen and Zhao (1998), Chen et al. (2000), Wang et al. (2009), Zhang et al. (2013) and Deng et al. (2015) to study the rock mass response to explosion loading. In their analysis, either LS-DYNA or AUTODYN was used in combination with UDEC to study the effect of the blast load on the surrounding rock mass. A common conclusion by these authors was that the approach was capable to model the blast load in a jointed medium with a reliable approximation.

In this paper, first the field Tests 1, 2, 4 and 5 are briefly described, and next the tests are numerically analysed using UDEC and LS-DYNA. At the end, the possible explanations for the issues raised after field Tests 1, 2, 4 and 5 are presented.

2. Review of Field Tests

The field Tests 1, 2, 4 and 5 were conducted in the completed production block 9 on the 741 m level in the Kiirunavaara underground mine. Tests 1 and 2 were conducted at the left- and right-hand side of cross-cut 93, and Tests 4 and 5 were conducted at the left- and right-hand side of cross-cut 95. The test design, summary of results, and the geological conditions around each cross-cut are presented in this section.

2.1 Design Summary (Tests 1, 2, 4 and 5)

A schematic diagram of the layout in Tests 1, 2, 4 and 5 are presented in Figure 1. The blastholes were drilled parallel to the cross-cut from the adjacent footwall drift. In all of these tests, except Test 4, two different charge diameters, were used to reduce the number of trials, i.e., the effect of two different blast loads could be investigated in each test. The blastholes were charged with NSP711. The dimension of the blastholes, charges and burdens in Tests 1, 2, 4 and 5 are summarized in Table 1. As the burden varied along the tested sidewall due to blasthole deviation combined with the irregular surface of the tested wall, only the average or effective burdens are listed in Table 1.

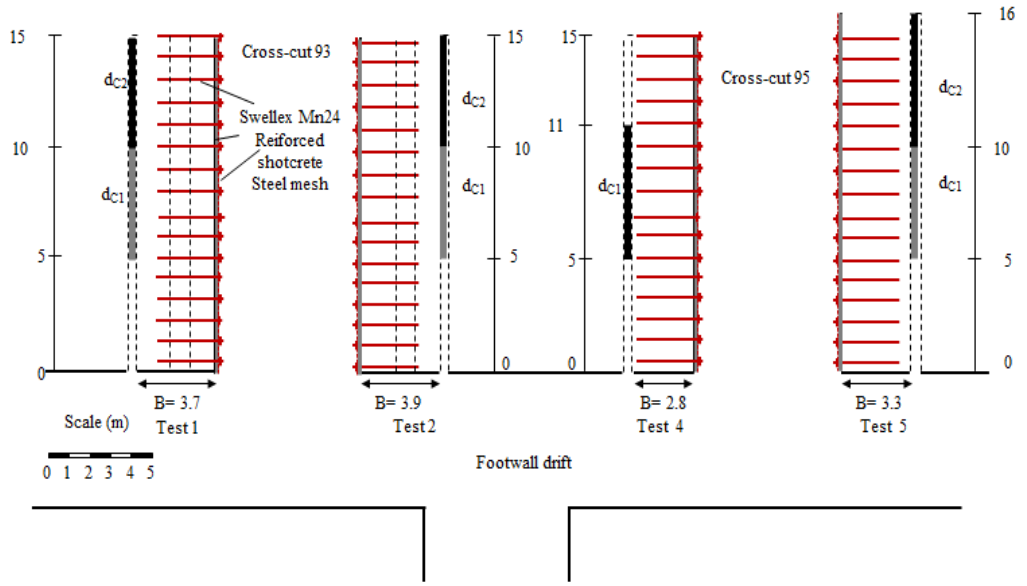

Figure 1: Schematic illustration of the tests layout in Tests 1, 2, 4 and 5 (Shirzadegan et al., 2016b).

Table 1: Burden, blasthole and charge dimension in Tests 1, 2, 4 and 5 (Shirzadegan et al., 2016b).

Test	Burden, B [m]	Blasthole diameter [mm]	Blasthole length [m]	Charge dia., d_{C1} [mm]	Charge length, d_{C1} [m]	Charge dia., d_{C2} [mm]	Charge length, d_{C2} [m]	Stemming (air) length [m]
1	3.7	125	15	45	5	76	5	5
2	3.9	152	15	76	5	98	5	5
4	2.8	152	15	120	6	---	---	5
5	3.3	152	16	94	5	83	6	5

A large number of accelerometers were installed and distributed over the test walls in Tests 1 and 2 and a few accelerometers were used to record the vibration level of the tested walls in Test 5. The accelerometers were installed at a depth of approximately 0.2 m from the free surface, for installation and protection purposes. In Test 2, four accelerometers were installed inside the burden (0.75 m and 1.5 m from the test wall) to measure the velocity and displacement at that depth. The accelerometers in Tests 1 and 2 were distributed along three rows and installed at the heights of 0.9 m (bottom), 1.8 m (middle), and 2.7 m (top) from the floor of the cross-cut. Three accelerometers were installed in Test 5, one at the low charge segment (1.8 m from the floor) and two at the high charge segment (2 m from the floor). A layout of the distribution of the instruments for example in Test 1 is presented in Figure 2.

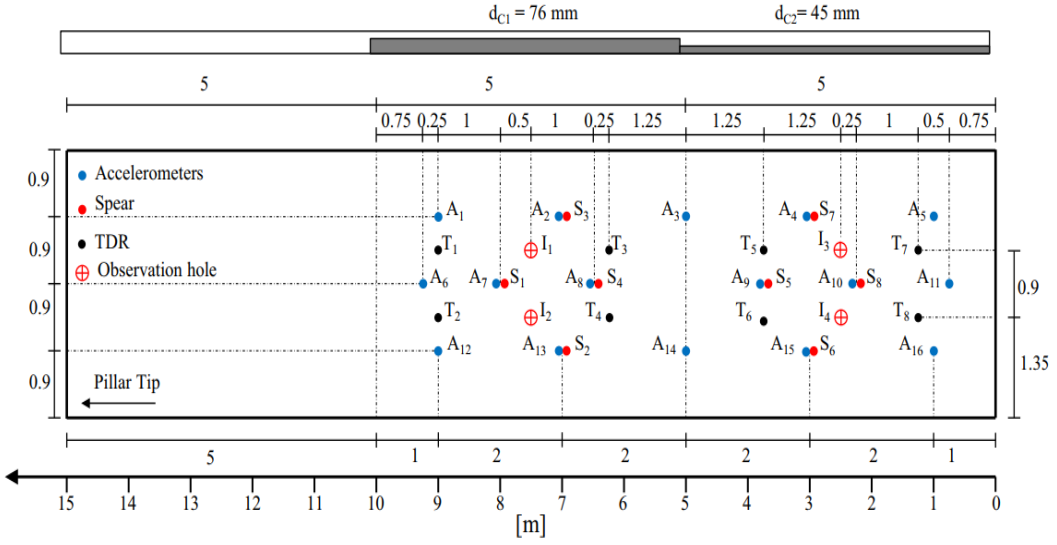

Figure 2: Distribution of monitoring instruments in Test 1 (Shirzadegan et al., 2016b).

The tested dynamic rock support consisted of 100 mm steel fibre reinforced shotcrete (40 kg/m^3 steel fibre), 75 mm × 75 mm weld mesh with 5.5 mm diameter, and Swellex Mn24 rockbolts with a length of 3 m and 1 m spacing installed in tested sidewalls in both crosscut 93 and 95.

Damage mapping of the tested walls were conducted after each blast. Post-blast observations of the tested support system in Tests 1 and 2 showed that cracks had been created on the surface of the reinforced shotcrete. No obvious damage to the rockbolts or the mesh was observed. Figure 3a shows an example of the cracks created on the surface of the shotcrete in Test 2. In Tests 1 and 2, the PPV was 6.5 m/s and 7.5 m/s, respectively. The damage observed on the tested walls and the rock support was almost negligible despite the high PPVs measured in these two tests.

Since the support system was only slightly damaged in Tests 1 and 2, the amount of explosive was increased in Tests 4 and 5. The increased charge concentration in Tests 4 and 5 resulted in a complete destruction of the burden. The ejection took place along the entire length of the charged portion of the blasthole. The ejected rock material in Test 4 was broken into rather small pieces, while in Test 5, the burden was broken into large blocks. Figure 3b shows the damaged burden in Test 5. Despite the complete damage of the burden, the data recording system satisfactorily registered the signals from the accelerometers in Test 5. The PPV in Test 5 at both charge segments was in the interval 6 – 7 m/s.

a) Test 2 **b) Test 5**

Figure 3: (a) Developed crack on the surface of shotcrete in Test 2 (b)destructed burden in Test 5 (Shirzadegan et al., 2016b).

2.2 Geological condition of the test sites

The geological investigation of the test sites was conducted by Andersson (2010). Eighty joints were mapped around cross-cut 93 where Tests 1 and 2 were conducted. The most significant set in cross-cut 93, was set 1 striking parallel to the cross-cut (Figure 4a). In cross-cut 95, 65 joints were mapped. Figure 4b shows that the dominating joint sets in cross-cut 95 were set 1, 2a and 3. According to Andersson (2010), the joint spacing in block 9 (cross-cut numbers starting with 9, e.g., 93, 95) generally lies in the range 0.5 – 2 m for most of the sets, but it may locally be denser. From Figure 4 (Andersson 2011), it is evident that for Tests 1 and 2 joint set 1 is dominant. However, there are 3 more sets, 2, 3 and 4 which are less frequently occurring (or observed during mapping). Moreover, joint sets 2 and 3 have two subsets with somewhat different strike and dip, denoted as a and b. For Tests 4 and 5, joint set 1 is the most dominant set, but 2a and 3 are also well-represented. Since joint set 2a in cross-cut 95 is almost perpendicular to the axis of the cross-cut, this set is not considered in the UDEC analysis. There is also one more joint set 4 which is less frequently occurring (or mapped).

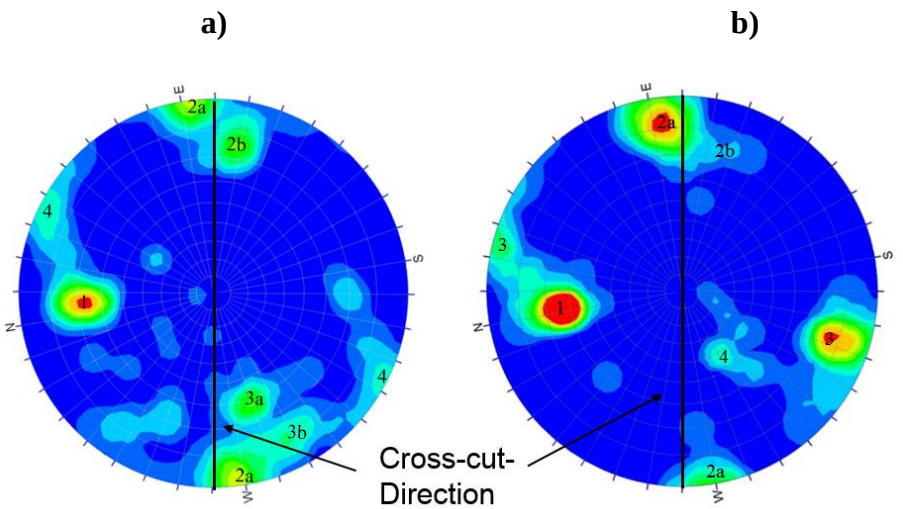

Figure 4: Joints orientation in the cross-cuts of a) Tests 1 and 2, and b) Tests 4 and 5 (Andersson 2011).

3. Numerical modelling technique

As UDEC has not the capability to simulate the blast load, this was done with the finite element program LS-DYNA. The created crushed zones around the blasthole absorb significant amounts of blast energy. However, this effect cannot be modelled in UDEC. Therefore, LS-DYNA was used to estimate the diameter of the crushed zone boundary (CZB) created around the blasthole due to the blast and to calculate the generated velocity of the CZB. The velocity-time function at CZB, calculated by LS-DYNA, was used as an internal boundary condition in the UDEC model.

3.1 LS-DYNA model

The initial stage of the blast in Tests 1, 2, 4 and 5 was simulated in LS-DYNA. The model featured a 10 m long explosive column with the diameter 76 mm for Test 1, 98 mm for Tests 2 and 5 and 120 mm for Test 4 in a blasthole with a length of 15 m. The diameter of the blasthole was 125 mm in Test 1 and 152 mm in Tests 2, 4 and 5. The detonation process was simulated by a three-dimensional model with the height of 25 m and a diameter of 20 m. Non-reflecting boundaries were applied around the outer boundaries of the model to eliminate the effect of wave reflections. The Jones-Wilkins-Lee (JWL) equation of state (Hallquist 2006) was used to model the explosive. The explosives were decoupled from the blasthole and the gap between the blasthole and the explosive was filled with air.

RHT material model was used in order to model the rock mass in LS-DYNA. RHT material model is an advanced plasticity model for brittle materials (Riedel et al., 1999) which is executed in LS-DYNA (Borrvall and Riedel 2011). The values of the parameters required for modelling of rock in LS-DYNA, including the uniaxial compressive strength, tensile strength, Poisson's ratio and Young's modulus, are listed in Table 3.

The RHT material model contains a damage model defined based on the continuum damage theory (Hallquist 2006). The crushed zone can therefore be calculated using the damage level, as the RHT material model can simulate compressive and tensile failures with the damage model. Figure 5a shows for example the calculated damage level around the blasthole in LS-DYNA for Tests 2 and 5. The red area around the blasthole in Figure 5a represents the crushed zone. The diameter of the crushed zone was 0.84 m for Test 1, 0.97 m for Tests 2 and 5, and 1.1 m for Test 4. The recorded velocity of the stress waves in the simulation of the four tests monitored at the CZB are presented in Figure 5b. In the LS-DYNA analysis of the field tests that had two different charge diameters, only the high charge segment was modelled.

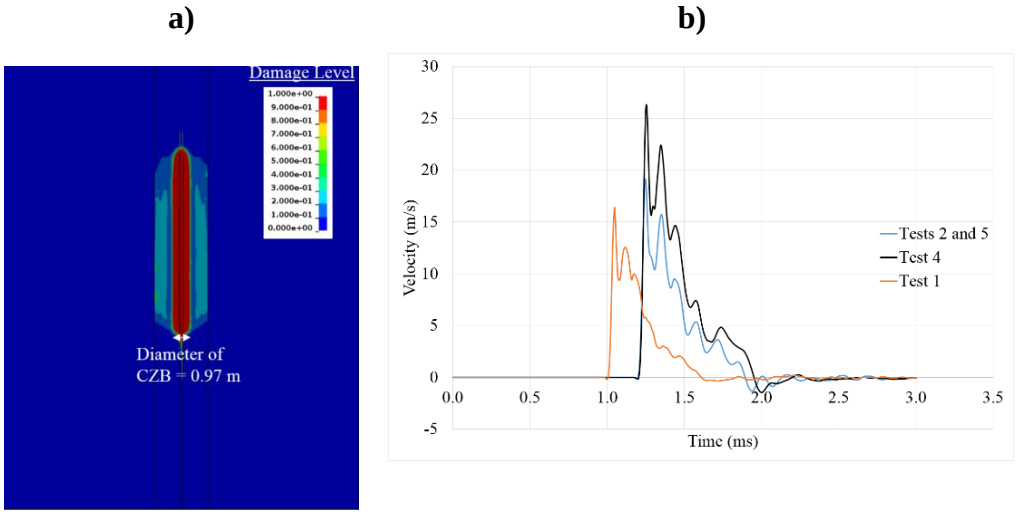

Figure 5: a) Identification of the crushed zone boundary in LS-DYNA model (Tests 2 and 5), b) Velocity at the crushed zone boundary.

3.2 UDEC models

Figure 6 shows the general configuration of the modelled geometry in UDEC. The external boundaries of the UDEC models were 80 m x 80 m, and the modelled cross-cuts were 7 m wide and 5.2 m high. Non-reflecting (i.e. viscous) boundaries were introduced around the outer perimeter of the domain to eliminate wave reflections. The identified dominant joint sets were explicitly modelled in the considered jointed region in Figure 6 and the velocity-time history at the CZB calculated by LS-DYNA for each blast design (different depending on the diameter of the blasthole and explosive), was used as an internal boundary condition at the CZB. Besides the geological conditions and the input velocity, another difference among the simulated tests was the burden, i.e. distance between the centre of the CZB to the test wall in Tests 1 – 5.

According to Deng et al. (2015), at least three layers of zones should lie between adjacent joints to balance between computational accuracy and efficiency. For this purpose, the zone edge length was set to 0.2 m to have at least three layers of zones between the considered smallest modelled spacing (0.6 m) between adjacent joints. The zone edge length of 0.2 m is smaller than the maximum recommended edge length by Kuhlemeyer and Lysmer (1973), i.e. 1/8 – 1/10 of the wave length λ, associated with the dominant frequency, to ensure the accuracy of the model.

The static stress applied to the model was 16.5 MPa along the *x*-direction and 11.3 MPa along the *y*-direction, representing the stress state at mining level 741 m (Malmgren and Sjöberg, 2006).

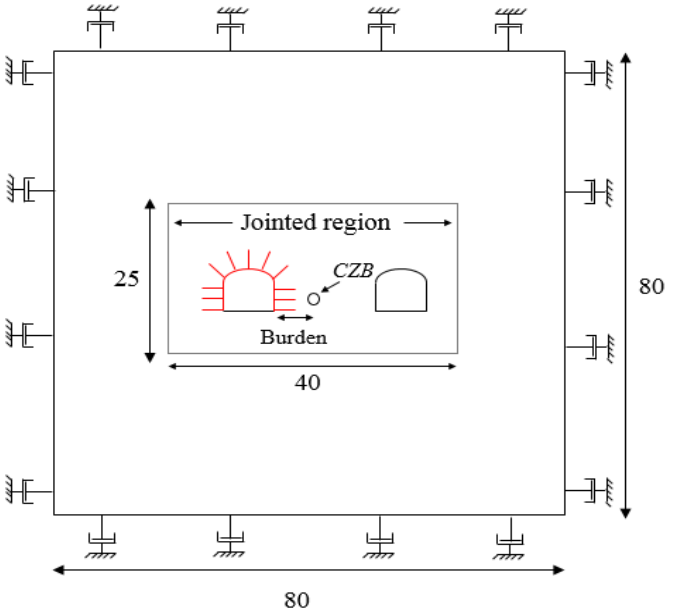

Figure 6: The geometry of simulation of the tests in UDEC model. Dimensions are in (m).

The material damping was not considered in the models. The reason was that the models comprised a joint set or two, that will cause the propagated wave energy to be absorbed by sliding along the joints and by the wave reflection at the joints (Deng et al., 2015). Furthermore, the Mohr-Coulomb perfectly plastic material model, which was used to model the rock blocks between the joints, absorb energy during plastic flow. A zero-material damping (for the blocks) was therefore assumed to be a good approximation of the conditions at the test sites for the parameter sensitivity analysis.

All the models were run for about 35 – 40 ms. This was the time during which the failure of the burden and the test walls were fully developed in the models. No further failure was developed in the area of interest after this cycling time.

Since UDEC is a 2D code, a number of assumptions had to be made when the models of Tests 1, 2, 4 and 5 were developed, i.e.

1. Only joints striking parallel to the crosscut were considered.
2. The joints were assumed to be persistent.
3. Only one joint spacing was considered for each model.
4. The block material between the joints could only yield, not break into smaller blocks.

As the joints were modelled in a two-dimensional program (UDEC), it was necessary to calculate the apparent dip of the joint sets modelled in UDEC. The following relation was used to calculate the apparent dip:

$$\tan \alpha = \tan \delta \times \sin \beta \qquad (1)$$

where δ is the true dip and β is the angle between the line of strike and the cross section of interest. The modelled joint orientations in UDEC for Tests 1, 2, 4 and 5 are presented in Table 2. In Table 2 the dip of each joint set is defined with a range of dips. Thus, the average value of the range is used to specify the true dip (δ) value.

Table 2: The major joint sets considered for modelling in UDEC in Tests 1 – 5.

Cross-cut	Test	Set	Dip [°]	δ [°]	β [°]	α [°]	Spacing [m]
93	1 and 2	1	55 – 80	67.5	86	67.5*	0.5 – 2
95	4 and 5	1	50 – 80	65	81	64*	0.5 – 2
		3	70 – 90	80	70	79.5	0.5 – 2
*The input angle in UDEC is 180 - α for the joint set due to their dip direction with respect to the test wall.							

3.2.1 Material properties

The used rock properties in UDEC are summarized in Table 3. The rock block was assigned intact rock properties as the joints were modelled explicitly. The parameters and their corresponding values were obtained from previous studies conducted by Malmgren and Nordlund (2008), Malmgren (2008) and Brandshaug (2009).

Table 3: Intact rock properties used in numerical analysis (Malmgren and Nordlund, 2008; Malmgren, 2008; Brandshaug, 2009).

Density [kg/m^3]	Elastic modulus [GPa]	Poisson's ratio	Bulk modulus [GPa]	Shear modulus [GPa]	Cohesion [MPa]	Friction angle [°]	Tensile strength [MPa]	UCS [MPa]
2800	70	0.27	50.7	27.6	31	61	16.5	267

The joint properties are summarized in Table 4. The presented data are based on previous studies conducted by Malmgren and Nordlund (2006). Small values were assigned to the tensile strength and cohesion of the rock joints to represent a virgin rock mass (Brandshaug 2009).

Table 4: Mechanical properties of the discontinuities (Malmgren and Nordlund, 2006).

Friction angle [°]	Cohesion [MPa]	Tensile strength [MPa]	Normal Stiffness [GPa/m]	Shear Stiffness [GPa/m]
35	0.5	0.5	9	9

3.2.2 Rock support properties

The mechanical properties of the reinforced shotcrete used in UDEC are summarized in Table 5. The properties are determined based on a series of laboratory tests conducted by Malmgren (2007). The second set of parameters that need to be specified to model the structural elements are the interface material properties. The mechanical properties of the interface are according to those determined by Saiang et al., (2005) and are listed in Table 6.

Table 5: Mechanical properties of reinforced shotcrete (Malmgren, 2007).

Density [kg/m^3]	Elastic modulus [GPa]	Poisson's ratio	Compressive yield strength [MPa]	Tensile yield strength [MPa]	Residual tensile yield strength [MPa]
2300	19	0.15	35	3.8	3.1

Table 6: Mechanical properties of shotcrete and rock interface (Saiang et al., 2005).

Normal stiffness [GPa/m]	Shear stiffness [GPa/m]	Cohesion [MPa]	Tensile strength [MPa]	Friction angle [°]
250	1	0.6	0.6	35

The geometrical specifications, mechanical properties, and the interface material properties of the Swellex bolt were according to a series of pull out test simulations in UDEC by Shirzadegan (2020), and technical specifications of Swellex and discussions with Epiroc, summarized in Table 7, Table 8 and Table 9.

Table 7: Geometrical specifications of Swellex Mn 24 (Shirzadegan, 2020).

Area [m^2]	Second moment of inertia [m^4]	Perimeter [m]
3.27×10^{-4}	11.06×10^{-8}	0.151

Table 8: Mechanical properties of Swellex Mn 24 (Shirzadegan, 2020).

Density [kg/m^3]	Elastic modulus [GPa]	Tensile yield load [kN]	Tensile failure limit
7800	200	240	0.35

Table 9: Mechanical properties of rockbolt and rock interface (Shirzadegan, 2020).

Normal cohesive strength [N/m]	Normal stiffness [N/m/m]	Shear cohesive strength [N/m]	Shear stiffness [N/m/m]
2×10^9	1×10^9	2×10^5	120×10^6

4. Numerical models calibration in Tests 1 – 5

The joint spacing around the cross-cuts where the field Tests 1, 2, 4 and 5 were conducted, were reported to vary between 0.5 and 2 m (Andersson 2010). Since the joint spacing is one of the factors that affects the calculated velocity on the surface of the opening, and the exact joint spacing within each set was not available, models of Tests 1, 2, 4 and 5 were analysed with the joint spacing 0.6 m, 1 m and 2 m. The reason for considering the smallest joint spacing as 0.6 m was to have at least 3 layers of the zones with length of 0.2 m between the joints to increase the computational accuracy.

The number assigned to the developed models, burden, number of joint sets, and the joint spacing in Tests 1, 2, 4 and 5 are summarized in Table 10.

Table 10: Model no., burden, number and spacing of joint sets used in the models.

Test	Model no.	Burden [m]	Number of joint sets	Joint set spacing [m]
1	1	3.7	1	0.6
	2			1
	3			2
2	1	3.9	1	0.6
	2			1
	3			2
4	1	2.8	2	0.6
	2			1
	3			2
5	1	3.3	2	0.6
	2			1
	3			2

In order to identify the model which shows the best agreement with the field data, the velocities and displacements calculated on the wall of the openings in UDEC models are compared with those obtained from the field tests. The model which has shown the best agreement with field data is chosen for further studies of the developed failure mechanism in the burden, and the rock support performance.

Tests 1 and 2 were conducted at the left and the right-hand side of cross-cut 93. Only one dominant joint set was observed during mapping of geological structures. Therefore, one joint set with orientation details presented in Table 2 was used in the simulation of Models 1, 2, and 3 of both tests. Figure 7 a and b show the models of Tests 1 and 2, with 0.6 m joint spacing. The analysis was repeated for the joint spacing 1 m and 2 m. The history points for recording velocity in the UDEC models of Tests 1 and 2, were located at the heights 2.7 m, 1.8 m, and 0.9 m from the floor. This is identical to the positions of the accelerometers used in the field test. In this paper, the measurements at the different heights are denoted "top" (2.7 m), "middle" (1.8 m), and the "bottom" (0.9 m) heights.

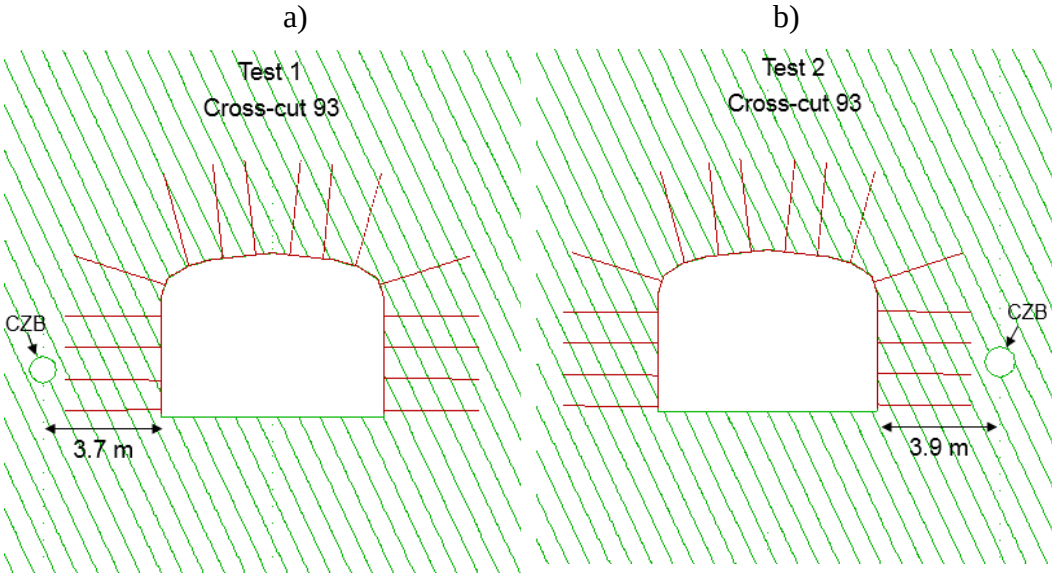

Figure 7: Simulated model in UDEC for 0.6 m joint spacing (Model 1) a) Test 1 and b) Test 2.

Tests 4 and 5 were conducted at the left and the right-hand side of cross-cut 95, respectively. From the field mapping, three dominant joint sets were identified for Tests 4 and 5. Since one of the dominant sets was perpendicular to the cross-cut direction, two joint sets with orientation details presented in Table 2 were used in the models of the tests. Figure 8a and b show the models with 0.6 m spacing for both joint sets. The analyses were repeated for the joint spacing 1 m and 2 m.
The history point for recording of the velocity in different UDEC models of Test 5, was located at a height of 1.8 m (middle) from the floor, identical to the position of the measurements in the field Test 5. Although no vibration measurement was conducted in field Test 4, in the models of Test 4, the velocity was monitored at a height of 1.8 m from the floor (middle).

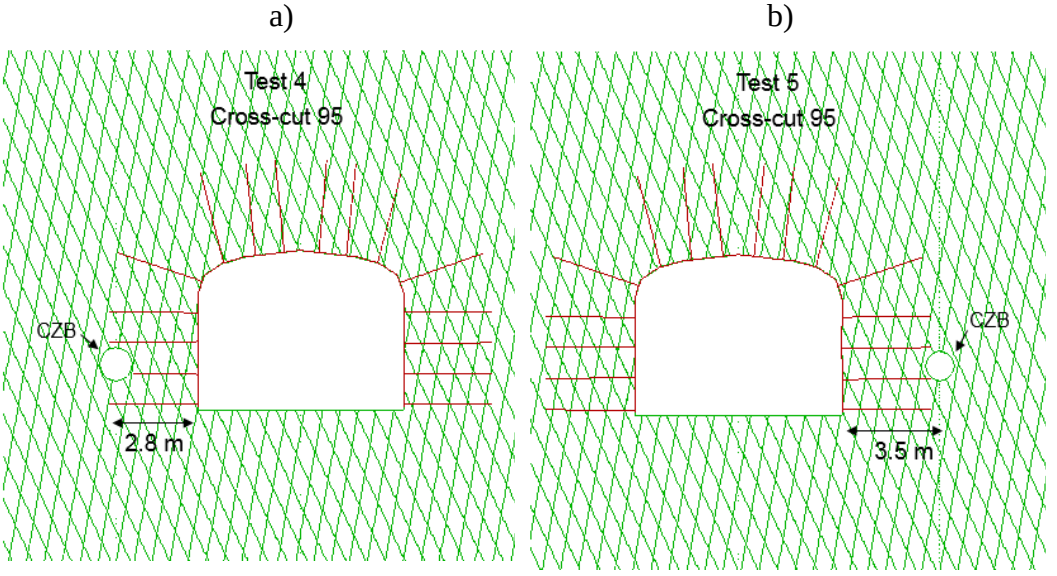

Figure 8: Simulated models in UDEC for 0.6 m joint spacing (Model 1), a) Test 4 and b) Test 5.

4.1 PPV comparison

In previous studies of combining LS-DYNA and UDEC or AUTODYN and UDEC, PPV was used to check the accuracy of the numerical models. This was done by comparing the numerically calculated PPVs to those measured in the field. Examples are the studies conducted by Deng et al. (2015), and Wang et al. (2009). In the present study, initially the PPVs calculated by UDEC models and those obtained from field measurements were compared to check the accuracy of the models and to find the model and jointing condition in each test that best represent the field test behavior. Table 11 summarizes the PPV measured during field tests and those calculated by different UDEC models. In this table, the field PPVs are those measured at the high charge segments. It should be noted that in Test 4 no accelerometer was used, therefore, only PPVs calculated with UDEC at the middle height is presented.

Table 11: PPV comparison between UDEC and field test measurements.

Test	Location of accelerometers (history points)	Calculated PPV from numerical models [m/s]			Calculated PPV from acceleration measurement from field tests at high charge segment [m/s]
		Model 1	Model 2	Model 3	
1	Top	5.5	3.4	3.3	5.0 and 5.3
	Middle	3.8	4.0	3.3	5.1 and 6.6
	Bottom	1.7	1.8	2.9	5.8 and 6.7
2	Top	2.4	2.3	3.1	2.4, 3.8, and 5.1
	Middle	5.2	4.6	3.9	5.2 and 7.5
	Bottom	5.2	4.1	4.6	5.8 and 6.1
4	Middle	11	8.3	8.9	No field measurement
5	Middle	6.1	6.1	5.2	7.0 and 7.1

From the results presented in Table 11 it can be observed that:

- In Test 1, the PPV calculated by Model 1 at the "top" is close to that recorded during the field measurement. At the rest of the heights in Models 1 – 3 in Test 1, lower PPV values are calculated compared to those measured in the field.
- In Test 2, all three models calculated PPVs within the range of the field measurements at the top. At the "middle" and "bottom", Models 1 and 2 have calculated PPVs close to that of the field measurements.
- In Test 5, all Models, 1, 2 and 3, calculated high PPV values, but the PPV from the models with 0.6 m and 1 m joint spacing (Models 1 and 2) were those closest to the field measurements.

In the present study, and according to the comparison of the PPV from the field test and those calculated by UDEC, it was clear that identifying the models that have well mimicked the real behavior of the field tests based on PPV is impossible.

4.2 Velocity-time comparison between field and UDEC

As PPV comparisons did not provide satisfactory results, in order to identify the numerical models which could represent the field tests in this study, the full velocity-time graphs calculated in UDEC were compared to those obtained from the field tests. The results associated with Test 1 are presented in Figure 9 Test 2 in Figure 10 and Tests 4 and 5 in Figure 11. Except in Test 4, in each plot, one or two velocity-time graphs obtained from the field tests are plotted together with the UDEC results. From the numerical model of Test 4, only the UDEC calculated velocities are plotted.

4.2.1 Test 1

The velocity-time graphs recorded during field Test 1 (Firure 9), show that, upon the arrival of the stress wave to the test wall, the particle velocity increases to a peak value. At the middle and bottom heights of the wall, the velocity mainly remains at a peak state for a duration of up to 4.0 ms. It is also evident that for some of the field velocity-time graphs, the peak occurs in the beginning, while for some accelerometers such as A7, A8 and A13 in Test 1, there are several peaks.
From the velocities calculated in Models 1, 2 and 3 in the models of Test 1 it can be observed that:

- At the top, the field velocity and that calculated by UDEC Model 1, agree well (Figure 9a).
- At the middle, the velocities calculated by Models 1 and 2, have a similar shape and duration as that recorded by accelerometers (A7 and A8) (Figure 9b). At this height, the field recorded velocities are slightly higher than that calculated by Models 1 and 2.
- At the bottom, no similarity can be observed between the UDEC and the field curves (Figure 9b).

According to the observed results, Model 1 with 0.6 m joint spacing corresponds slightly better with the field test behavior.

a)

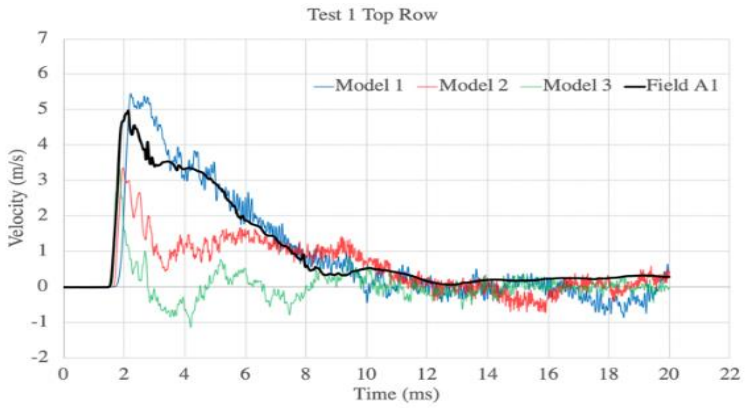

b)

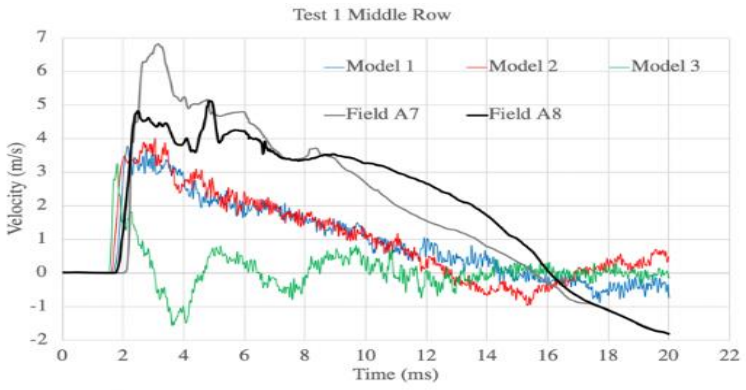

c)

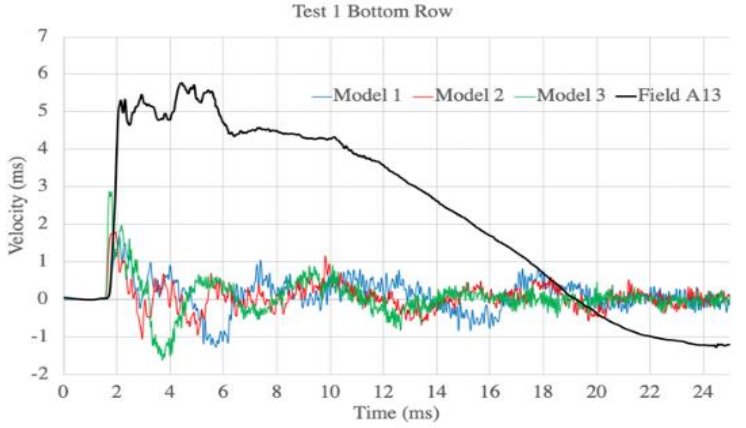

Figure 9: Velocity-time comparison between UDEC and field measurements in Test 1, a) top, b) middle, and c) bottom.

4.2.2 Test 2

From the velocity-time curves calculated in the models of Test 2, it can be observed that:

- At the top, the trend in Model 1 is similar to that of the velocity measured in the field by accelerometer A2, but the velocity calculated by Model 1 has a shorter duration and a lower amplitude (Figure 10a).
- At the middle height, the results from Model 1 is most similar to that recorded by A9 (Figure 10b). The velocity calculated by Model 2 is somewhat lower and the duration is shorter than that calculated by Model 1.
- At the bottom, the agreement between field and Model 1 is less good (Figure 10c).

From the velocity results observed in different models of Test 2, it was concluded that Model 1 with 0.6 m joint spacing has provided results closest to that observed in the field Test 2.

a)

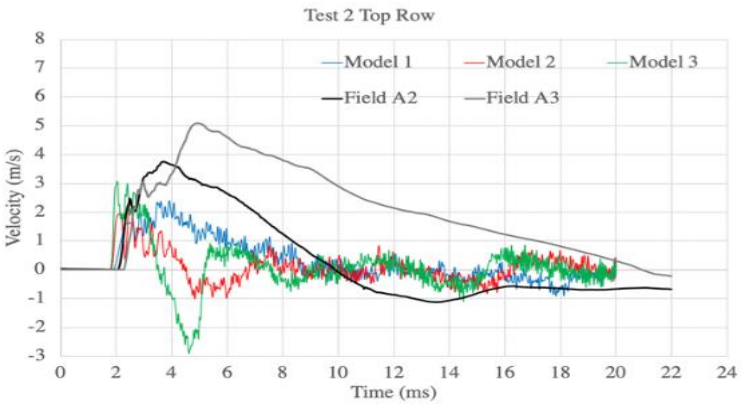

b)

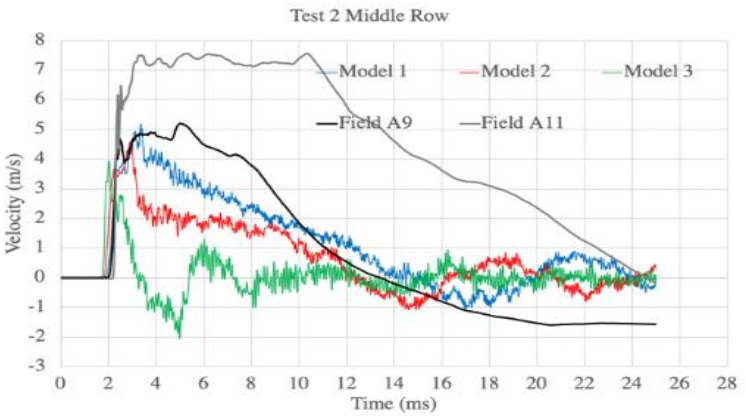

c)

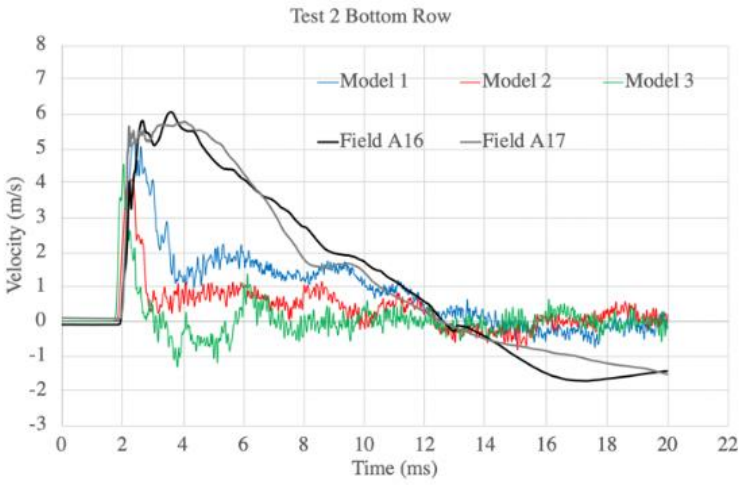

Figure 10: Velocity-time comparison between UDEC and field measurements in Test 2, a) top, b) middle, and c) bottom.

4.2.3 Tests 4 and 5

As no accelerometer was installed in field Test 4, only the velocity-time curves calculated in UDEC (in the middle of the wall) are used to study the response of the opening to the blast-induced wave. The calculated velocities in the models of Test 4 are presented in Figure 11a. All three models have shown similar response, but higher velocity was calculated in Model 1. The lack of deceleration to a zero velocity, calculated in UDEC, indicate the ejection of rock blocks from the test wall in all Models 1 – 3. The burden in Test 4 was fully destructed after the blast.

In Test 5, despite the burden was fully destructed after the blast, the accelerometers recorded the ground vibration satisfactorily. The velocity-time curves obtained from field Test 5 and those calculated in the Models 1 – 3 are presented in Figure 11b. The velocity calculated by Models 1 and 2 are similar to that recorded by accelerometers A1, A2 and A3, around the peak. The UDEC Model 3, shows a deceleration similar to that of accelerometer A3, but the duration around the peak is shorter than that obtained in the field. Since the burden in Test 5 was fully destructed, the velocities calculated by Models 1 and 2 are more similar to the velocities recorded by the accelerometers (and integrated one time with respect to time) in the field.

From the velocity-time graphs presented in Figure 11 for Tests 4 and 5, and considering the fact that these two tests were conducted at the left and right hand side of the same cross-cut, it can be concluded that both Models 1 and 2, with a joint spacing range between 0.6 – 1 m, corresponds well to the behaviour of field Tests 4 and 5.

a)

b)

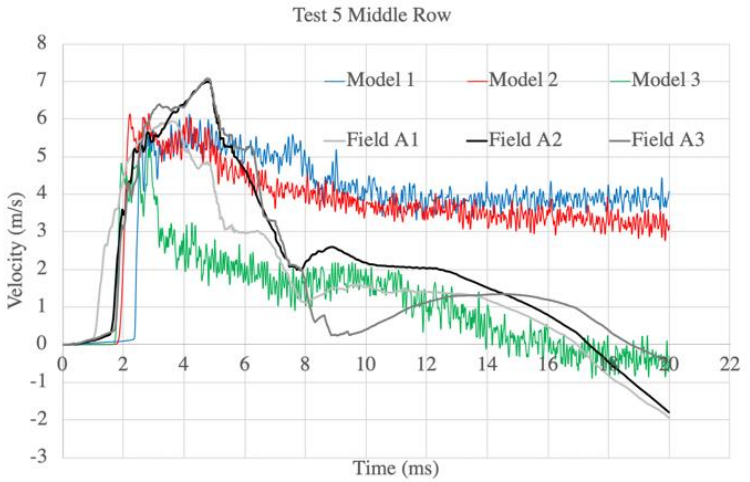

Figure 11: Comparison of velocity-time curves a) in UDEC models in Test 4, and b) between UDEC models and field measurements in Test 5.

4.3 Displacement and ejection thickness

The maximum displacement, and the ejected thickness of the blocks of rock in Model 1 of Tests 4 – 5 are shown in Figure 12a-d. The displacements calculated in the models are obtained from the displacement after 40 ms of wave propagation and were the maximum displacements calculated over the height of the wall.

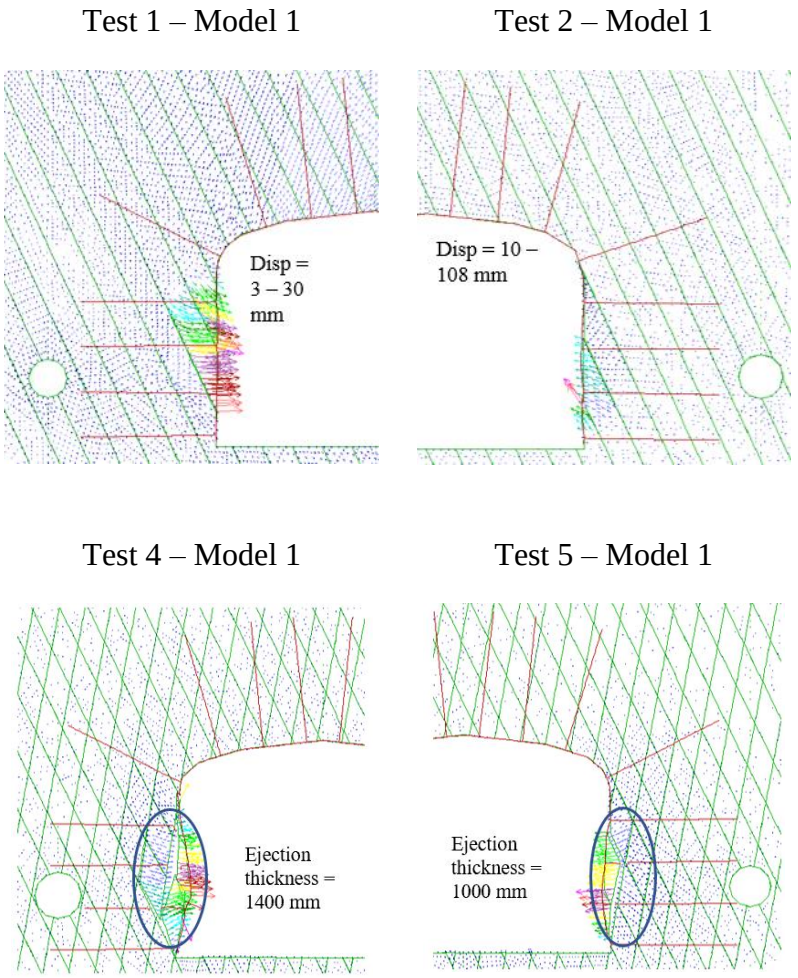

Figure 12: Displacement of the test wall in the simulated models a) Test 1, b) Test 2, and ejection thickness in c) Test 4 and d) Test 5.

The maximum displacement of the test wall, and the ejection thickness, measured in the field tests are summarized in Table 12. The comparison of the displacements measured in the field, and those calculated by the models of Tests 1, 2, 4 and 5, shows that the results from Models 1 fall within the range of the field measurements for all tests.

The summary of the calculated displacements in Table 12, for Tests 1 and 2, shows that Model 1, can represent the field behavior and is well suited to use when addressing damage and rock support performance.
In field Tests 4 and 5 it was not possible to measure the displacement of the wall as the burden was fully ejected. However, the numerical analysis of these two tests indicate a large failure thickness of the wall and the burden, which is in line with the level of damage observed in these two tests.

Table 12: Displacement, and ejection thickness of the wall in the numerical models and field measurement of Tests 1, 2, 4 and 5.

Test	UDEC model	UDEC disp. (mm)	Field disp. (mm)	UDEC ejection thickness (mm)	Field ejection thickness (mm)
1	1	3 – 30	6 – 71	-	-
	2	3 – 28		-	
	3	0 – 8		-	
2	1	10 – 108	2 – 110	-	-
	2	3 – 32		-	
	3	1 – 13		-	
4	1	-	-	1400	2800 (burden)
	2	-		700*	
	3	-		700	
5	1	-	-	1000	3300 (burden)
	2	-		500	
	3	-		0	
* due to computational errors, only results up to 17 ms cycling time are available					

5. Behaviour of the rock mass in the burden after blasting

The failure process in the burden is studied by checking the plasticity state of the models. This was done to evaluate the burden design in Tests 1 to 5 and to find the reason for the low level of damage in Tests 1 and 2, and the total burden destruction in Tests 4 and 5.

Figure 13a-d shows the failure developed in the burden of the models. The zones yielded in tension in the burden are used as indicators of the location of the created fractures in the burden.

The zones yielded in tension are mainly distributed in three sections of the burden (i) around the CZB, (ii) in the middle of the burden, and (iii) in the wall of the cross-cut.

The tensile yielding around the CZB in section (i) is developed in all of the models of Tests 1 – 5, as a result of the initiation of the wave propagation in that section.

The main difference among the models was in the middle (section (ii)) and close to the surface of the test wall (section (iii)) where the zones yielded in tension developed differently in different models.

More zones in section (ii), are yielded in tension in the analyses of Tests 4 and 5 compared to that in Tests 1 and 2. The zones yielding in tension in the models of Tests 4 and 5, are propagated from the CZB outward in all directions, while in Tests 1 and 2, a thin layer of zones yielded in tension, can be observed in the middle of burden, and the yielded zones are not as extensive as in Tests 4 and 5.

In section (iii), the area yielded in tension on the test wall surface in Test 1, is located in the upper part of the wall, while in Test 2, the lower part of the wall has yielded in tension. This can be due to the orientation of the joint set with respect to the wall in each model. In the models of Tests 4 and 5, the yielded zones are distributed all over the height of the test wall.

From the presented results, it can be concluded that in field Tests 4 and 5, the tensile yielding zones starting from the CZB and extending toward the wall surfaces, has dominated the failure of the burden. In the model of Test 4, most of the zones in the burden are yielded in tension. In the model of Test 5, tensile yielding is also evident, but the area with yielded zones is less extensive than that in the model of Test 4, especially in the rock mass between the CZB and the shoulder. The reason is due to the higher amount of explosive material combined with a smaller burden in Test 4 than in Test 5. In the models of Tests 4 and 5, the separation of wedges which were formed close to the surface opening, is clear. However, the depth of the ejection is more limited than that observed in the field (where the whole burden was ejected). The failure of the walls in Tests 4 and 5 is not limited to a typical wedge but consisted of several blocks which translate and rotate.

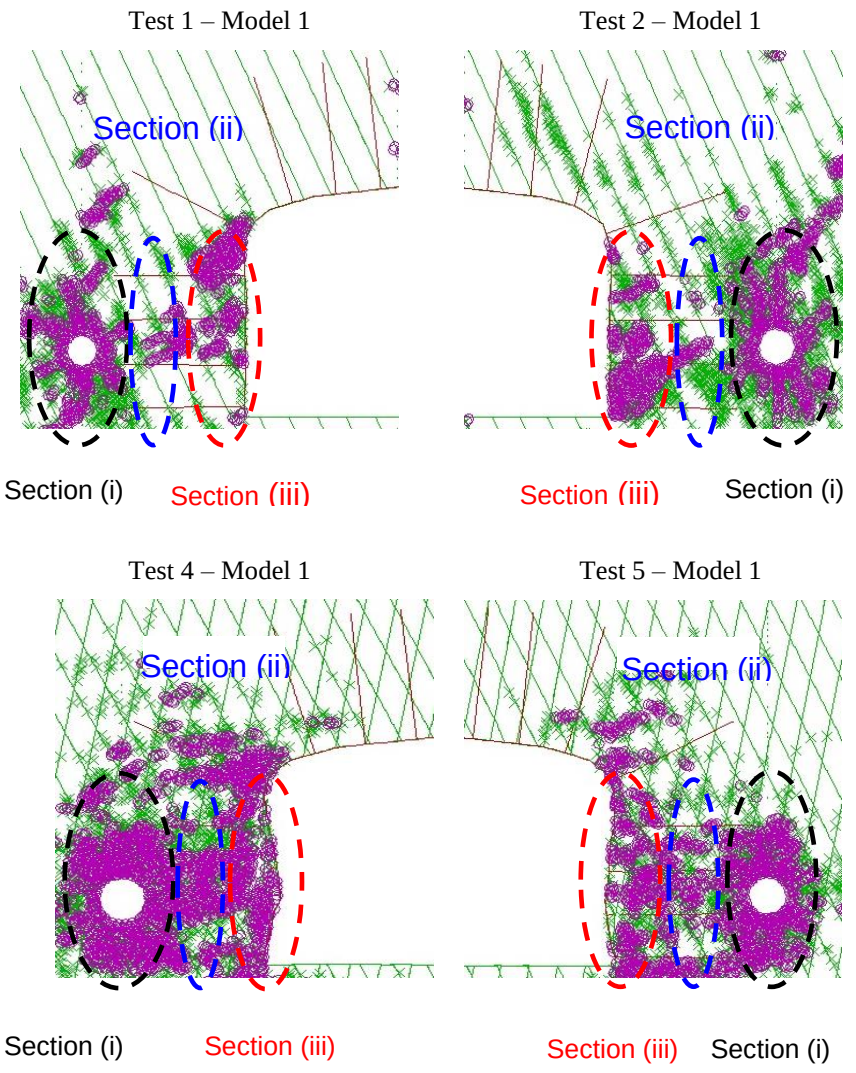

Figure 13: Tensile yielding and fractures developed in the burden of the models in a) Test 1, b) Test 2, c) Test 4 and d) Test 5.

6. Rock support performance

The loading state and the failure developed along the rockbolts and in the shotcrete in Tests 1, 2, 4 and 5, are investigated numerically, and the results are presented in the following sections.

6.1 Rockbolt performance

6.1.1 Breakage

In UDEC, a Rockbolt element is considered as a linear elastic material initially that may yield in the axial direction, i.e. tension or compression (Itasca Consulting

Group 2015). Furthermore, inelastic bending can be simulated in Rockbolt elements by identifying a limiting plastic moment. This provides the possibility to calculate the axial and bending plastic strains of the simulated bolt. The strength of the Rockbolt elements is defined at its nodal points by specifying a tensile failure strain limit (defined by the user). If the total calculated strains (axial and bending) exceed the user defined tensile failure strain limit, bolt breakage will occur at the nodal points (Itasca Consulting Group 2015). In this section, the loading state and the induced strain in the bolts in the numerical models of Tests 1, 2, 4 and 5 are studied. The rock bolts closest to the blasthole in the models of Tests 1 – 5 showed an axial force of 240 kN (equal to the pre-defined tensile yielding limit) after 3 ms of wave propagation.

The rockbolt breakage state in the models of Tests 1, illustrated in Figure 14a, showed that despite the high axial loads on the rockbolts, no rockbolt breakage occurred. This was in line with the level of damage to the rockbolts observed during field Test 1, where no sign of ejection/breakage of the rockbolts was observed after he blast.

In Test 2, the third rockbolt from floor showed breakage at the element closest to the surface of the opening (see Figure 14b). Despite the rockbolt breakage in the model of Test 2, the integrity of the support system is maintained, and no obvious ejection from the wall of the model can be observed. Similarly, in field Test 2 no signs of ejection from the wall was observed during damage mapping of the test wall. Furthermore, no clear evidence of the breakage of the rockbolts was found. One explanation for the breakage of the bolt in model of the Test 2 is the possible difference in formation of critical wedges or rock blocks very close to the surface of the opening between the field test and the model. The breakage of the bolt in model of the Test 2 is because the bolt intersects the joint and large movement along the joint has occurred.

a) Test 1 b) Test 2

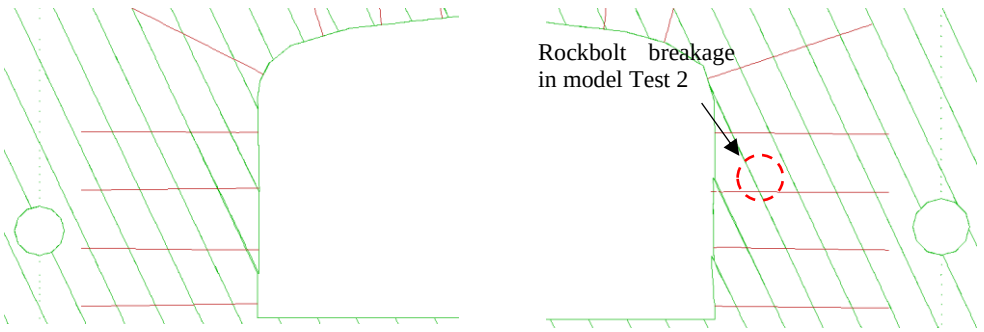

Figure 14: Rockbolts breakage state in a) Test 1, and b) Test 2.

Figure 15a and b show the state of the rockbolts for Tests 4 and 5. Rockbolt breakage can be observed close to the surface of the opening where the outermost parts of the rockbolts are moving together with the blocks which are detached from the rock mass. The rockbolts broken close to the surface of the opening were at the length between 0.1 – 0.6 m in the numerical models of Tests 4 and 5. This is the length of the rockbolt which is ejected from the wall due to the stress wave reflection. Since the burden in Tests 4 and 5 were fully destructed, the rest of the remaining length (2.0 – 2.5 m) of the bolt in the burden, is ejected in the next phase due to the expansion of blasting gases.

Mapping of the ejected rockbolts after the blast in field Tests 4 and 5, showed that some of the rockbolts were broken into small pieces with lengths in the interval 0.5 – 1 m. Mapping of the rockbolts in the field also showed that the rockbolts were ejected and broken into pieces with lengths of 2 – 2.5 m (see Figure 14c). This was in line with the observed rockbolt breakage in the numerical analysis of the Tests 4 and 5.

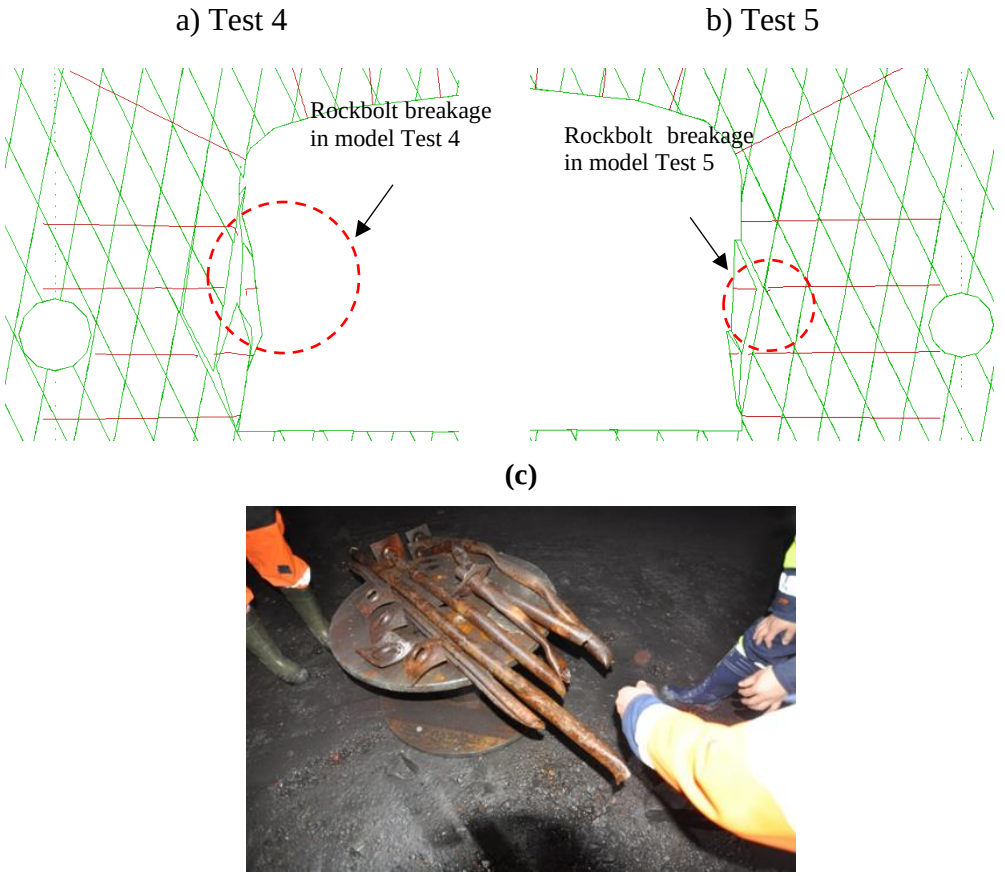

Figure 15: Rockbolt breakage in a) model of Test 4, b) model of Test 5, c) field tests.

6.1.2 Rockbolt/rock interface failure

The behaviour of the rockbolt/rock interface in UDEC is dependent on the normal and shear behaviour at the rockbolt nodal points. If the developed shear and normal forces exceed the maximum shear or normal force of the interface (the strength of the interface), the interface in the axial and normal direction will fail.

Figure 16a and b shows the failure developed at the interface between the rock and the rockbolts in Tests 1 and 2, respectively. The failure mainly developed in the three rockbolts closest to the blasthole. The maximum length of the failed section in one of the rockbolts in Test 2 was around 1.5 m (the full rockbolt length was 3 m). For the rest of the rockbolts in Tests 1 and 2, a few shorter interface failures could be observed. This indicates that the major length of the rockbolts have not lost their functionality and are still connected with the surrounding rock mass. During field Tests 1 and 2, no sign of breakage of the rockbolts or ejection from the tested walls were observed.

Figure 16c and b shows the associated interface failure in the rockbolts in Tests 4 and 5. In Test 4 (Figure 16c) the interface failure developed along the whole length of the four rockbolts at the side of the blasthole. In Test 5 (Figure 16d), interface failure occurred along whole length of the two rockbolts close to the blasthole and parts of the lengths of the two other rockbolts.

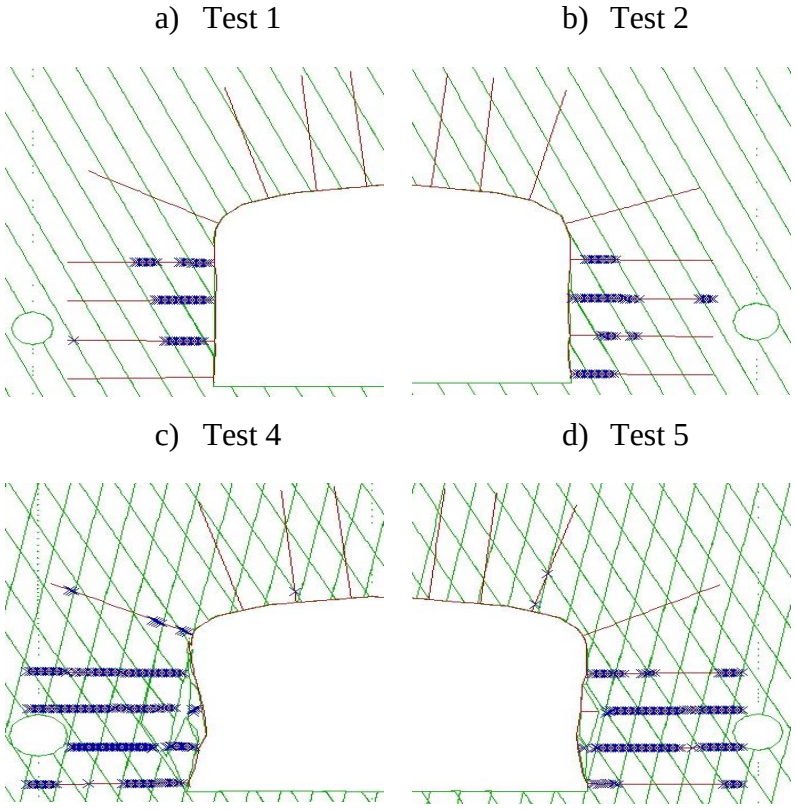

Figure 16: Rockbolt interface failure in a) Test 1, b) Test 2, c) Test 4 and d) Test 5.

6.1.3 Rockbolt energy absorption

Shirzadegan et al. (2016a) calculated the energy absorption by one of the rockbolts in field Test 2. The deformation induced to the rockbolts during the numerical analysis of Test 2, was used to estimate the energy absorption by the rockbolts and was compared with the results from the field tests.

The displacement of the nodal points of the rockbolts in the model of Test 2 is illustrated using bar graphs (Figure 17a). These plots show drastic changes in nodal displacement along rockbolts 2 and 3, indicating localized elongation/strain. The nodal displacement along the other rockbolts (1 and 4), are more evenly distributed. The total elongation of rockbolt 2 was 21 mm. As indicated in the figure, rockbolt 3 failed close to the cross-cut wall. Maximum 30 mm elongation was observed before the bolt breakage.

The total elongation of the elements was then related to the energy absorption curve of the Swellex Mn24 obtained from a series of laboratory tests conducted by Voyzelle et al. (2014), presented in Figure 17b. In total, close to 5 kJ was absorbed by the elements of rockbolt 2, and 7 kJ by rockbolt 3 in the UDEC analysis of Test 2. A similar approach was used by Shirzadegan et al. (2016a) to calculate the energy absorption by one rockbolt in Test 2 (field test). The second integration of the accelerometer readings was used to calculate the rockbolt elongation. An energy absorption of 17 kJ, i.e., higher than that obtained from the numerical analysis of Test 2, was obtained.

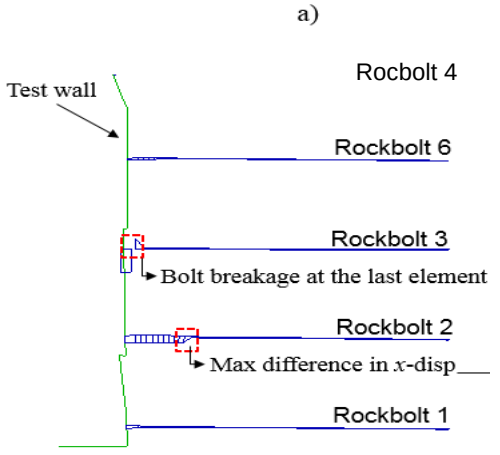

(b)

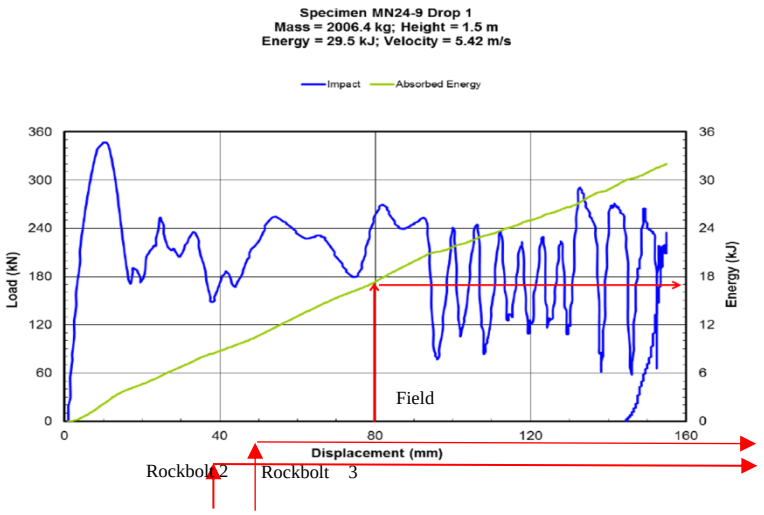

Figure 17: a) Identification of the most elongated rockbolts in Test 2, b) total energy absorption by rockbolts 2 and 3, and the bolt installed in the field (original energy absorption graph by Voyzelle et al. (2014)).

6.1.4 Shotcrete performance

Rock/shotcrete interface failure, and axial yielding of the shotcrete were the main yielding modes that were detected in the models of Tests 1 and 2. The plots associated with the shotcrete axial (tensile) yielding and interface failure are presented in Figure 18a and b respectively. The plots represent the status after 3 ms of wave propagation (from CZB) in the model. The numerical analysis results indicate that, upon the arrival of the wave at the tested walls, the shotcrete/rock interface failed. After 40 ms, 84 mm of residual displacement (in *x* direction) was calculated in the model of Test 2. In the numerical analysis of Test 2, the relative displacement between the rockbolts and the shotcrete (in *x*-direction) is calculated to estimate the maximum residual deflection of the shotcrete after the dynamic loading, see Figure 18c. Rockbolts 1 and 2 showed a maximum displacement of 9 mm and 21 mm, respectively. Therefore, an average displacement of 15 mm was considered to be subtracted from the shotcrete maximum displacement. This resulted in 69 mm of deflection of the shotcrete.

Thyni (2014) performed a series of round panel tests to measure the energy absorption by the reinforced shotcrete. The energy absorption graph for a panel of 100 mm thick reinforced shotcrete obtained by Thyni (2014) is according to Figure 18d. The calculated deflection in the numerical analysis of Test 2 is related to the energy-deflection graph presented in Figure 18d. For the deflection of 69 mm, the maximum energy absorption by the shotcrete calculated based on the results from the numerical analysis of Test 2 was 2.6 kJ. The energy absorption calculated from the field test results and from the UDEC energy analyses is shown in Figure 18d.

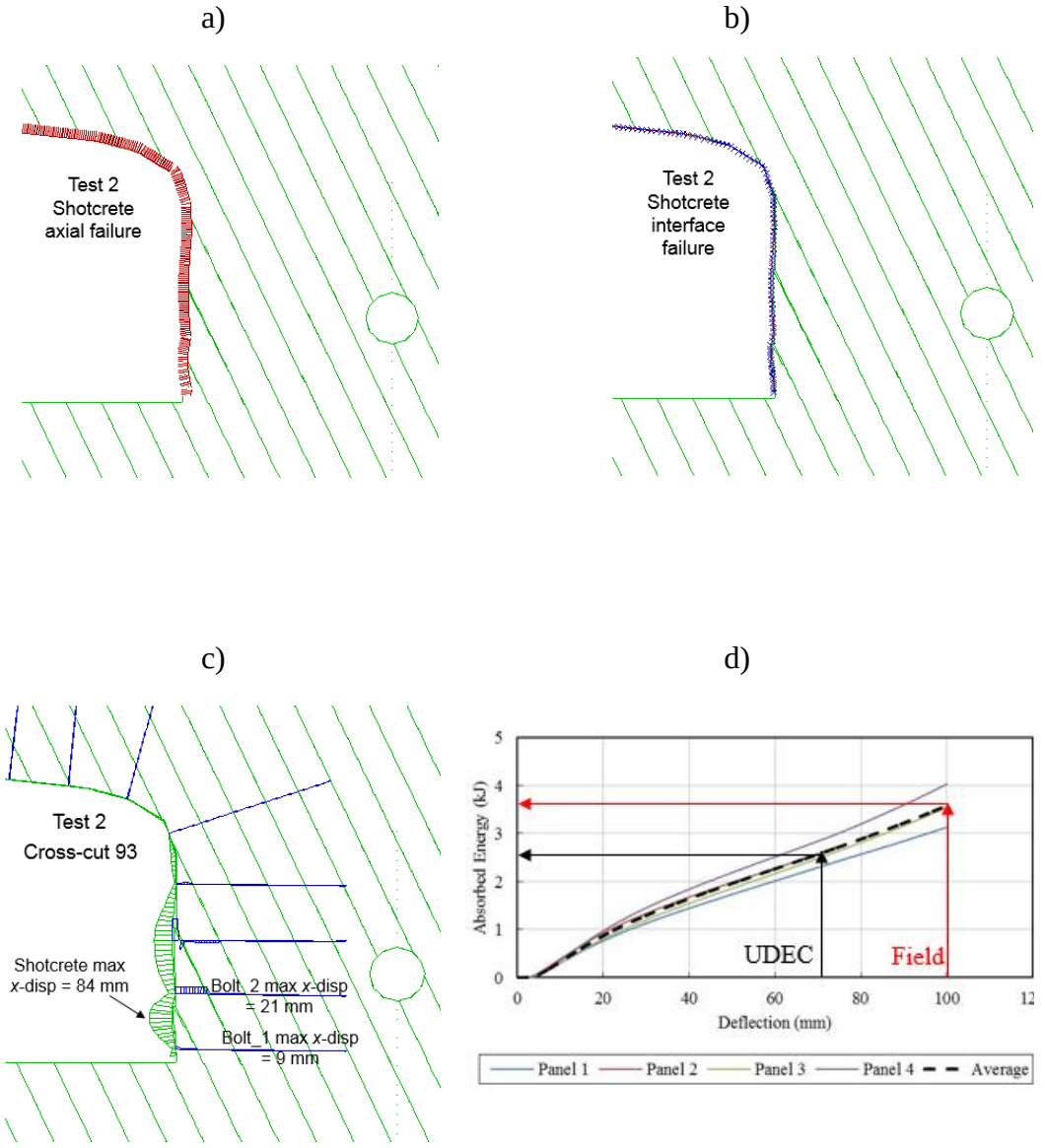

Figure 18: a) Shotcrete axial failure, b) shotcrete interface failure, c) shotcrete deflection, d) shotcrete energy absorption (Thyni, 2014).

7. Discussion of results

Several UDEC models were developed and used for analysis. To identify the models that best represent the behaviour of field Tests 1 – 5, PPV, velocity-time graphs, maximum displacement generated on the test wall, were used to compare the field tests results and the model results.

7.1 Comparison between field tests and numerical models

The difference between the PPV obtained from numerical models and field tests, showed that PPV alone could not be used to identify the models that best mimics the real rock mass response. Therefore, velocity – time graphs calculated at the surface of the wall by the numerical analysis were compared to those measured in the field. The similarities in general trends of the velocity – time graphs obtained from the field tests and those calculated using UDEC, was used to identify the models that can represent the field tests. Further comparison of the displacement of the wall, confirmed that the chosen models mimics well the failure mechanism in the burden and the response of rock support to the stress wave.

One reason for the velocity (and also PPV) differences between field tests and numerical models, is the geological structures in the burden. In the presented UDEC analysis, the dominant joint sets, which have a strike parallel to the direction of the cross-cuts were modelled. The dominant joint sets with strike perpendicular to the direction of the cross-cuts, together with other existing, but less frequently occurring sets and subsets, are excluded from the 2D modelling. Obviously, the combination of the dominant sets together with the less frequent joints can form local 3D wedges in the wall. This can cause local sliding and separation along the joint planes along the test wall. This means that the rock mass in the tested wall can be locally more complex than that modelled in UDEC, and that 3D wedges of different size, formed by different combinations of joint sets, may have existed in the wall. Each individual wedge and each additional joint in the wall, may have affected the response and may be the reason for the differences between that recorded by different accelerometers in the field tests, and those calculated by UDEC.

7.2 No ejection in Tests 1 and 2 despite of high PPV

The numerical analysis of the tests provided answers to the questions raised after performing the field test. During Tests 1 and 2, no rock ejection (similar to that in actual seismic event) occurred from the wall of the cross-cut and the level of damage to the test wall and support system was minimal. Nevertheless, high PPVs were measured on the surface of the test walls.

In the numerical models of Tests 1 and 2, PPV values up to 5.5 m/s was calculated on the surface of the wall, similar to that in the field tests, but no ejection from the test wall was observed in the models. One reason shown by the numerical analysis of the tests, was the presence of only one dominant joint set in the burden around the site of the Tests 1 and 2. The presence of a larger number of joint sets in the vicinity of the test wall surface, will increase the probability that other wedges can

be formed and ejected.
The numerical analysis of Tests 1 and 2, showed that the tensile failure zones in the middle part of the burden, was limited to a thin layer of the zones. Shirzadegan et al. (2016a) measured the gas pressure in the burden in Tests 1 and 2. It was concluded that, the level of gas pressure was significantly reduced in the vicinity of the wall. The combination of a burden which is only lightly damaged and the low gas pressure resulted in a stable wall.

7.3 Failure mechanism developed into the burden in Tests 4 and 5

The numerical analysis of the tests also provided answers to the questions why the burden in Tests 4 and 5 was fully destructed, while the burden was almost the same as that in Tests 1 and 2.
The fact that the burden was completely destroyed in Tests 4 and 5, while it was stable in Tests 1 and 2, implies that the behavior of the rock mass was significantly different. One major difference between the test sites, was that there was only one major joint set striking sub-parallel to the cross-cut in 93 (Tests 1 and 2), while two joint sets were striking parallel to cross-cut 95 (Tests 4 and 5). The numerical analysis showed that the failure process of the burden in Tests 4 and 5, involved two steps. The first step, observed in the numerical analysis of the tests, was complex and involved several blocks between the wall and the middle parts of the burden, that were sliding and rotating outward into the opening upon the arrival of the stress wave. The second step occurred when the burden was ejected (in the field tests). The numerical analysis of Tests 4 and 5 showed that the incident stress wave induced extensive radial fracturing in middle section of the burden. These radial fractures were caused because the tangential tensile stresses induced at the incident wave front exceeded the tensile strength of the rock mass. The explanation to the ejection is that the extensively fractured burden was ejected due to the expansion of blasting gases in the middle sections of the burden.

7.4 Rock support performance

The response of the rockbolts to the dynamic loading in the UDEC models, was similar to that in the field tests. This means, that the integrity of the support system was maintained, and the level of damage to the rock support in the models was similar to that obtained in the field Tests 1 and 2. Moreover, no ejection of rock between the installed rock bolts occurred. The numerically calculated elongation and energy absorption by the rockbolt and shotcrete in Test 2, was smaller than that measured in the field tests. One reason can be due the elongation measurements in the field test. The displacement calculated from the field test is from the rock mass close to the installed rockbolt. Therefore, it can be assumed that the displacement of the collar of the rockbolt calculated in numerical analysis could be less than that measured in the field. This can also be due to the difference in the number of joint sets in the real cross-cuts and those modelled in the numerical analysis. Since UDEC is a 2D code, the structural geology has to be simplified, and only the joints striking

sub-parallel to the cross-cut can be modelled explicitly in the numerical analysis.
In Tests 4 and 5, the rockbolt breakage, and the rockbolt – rock mass interface failure, was developed almost along the whole length of the rockbolts closest to the CZB. Based on the results from the numerical analysis of Tests 4 and 5, the following process explains the failure mechanism developed in the rockbolts in the field tests:

1. The tensile radial stress induced by the reflected wave, caused rockbolt breakage at a distance of up to 0.6 m from the surface of the opening.
2. The segments of the rockbolts, closest to the cross-cut wall, were ejected together with formed wedges in the vicinity of the test wall surface.
3. The remaining portion of the rock mass was extensively fractured by the tensile tangential stress induced by the incident wave and the tensile radial stress of the reflected wave. This provided a path for penetration of gas into the burden.
4. The remaining length of the rockbolts in the rock mass, was ejected together with the remaining portion of the fractured rock in the burden as a consequence of the gas expansion. Field mapping of the ejected rockbolts showed that the length of the rockbolt pieces found was similar to that obtained in the numerical analyses.

8. Conclusions

The numerical analysis of four large-scale dynamic test of rock support (Tests 1, 2, 4 and 5) that were conducted at LKAB Kiirunavaara mine, have been carried out and the important conclusions were:

- The numerical models were able to mimic the behaviour of the jointed rock mass and the rock support fairly well. The difference in behaviour between the numerical models and the field tests, appeared to be caused by the gas expansion in the field tests, especially Tests 4 and 5. Since the burden was heavily damaged by the incident and reflected waves, the gas expansion could eject the broken rock and rock support. This was not possible to simulate in the numerical models. Even though the failure mechanisms were different, in different tests, the models produced realistic failure development in the tested walls.
- The numerical analysis of Tests 1 and 2, provided answers to the behaviour of the rock mass in field Tests 1 and 2. It is concluded that the number of major joint sets was the main reason to the difference between the failure development in Tests 1 and 2 and Tests 4 and 5. In Tests 1 and 2, only one joint set was striking sub-parallel to the axis of the cross-cut, compared to 2 major joint sets in Tests 4 and 5.
- The numerical analysis of Tests 1 and 2, confirmed the conclusion made during field Tests 1 and 2 (Shirzadegan et al. 2016a), regarding the minimum gas pressure in the vicinity of the test wall in those tests. Only a thin layer of zones,

yielded in tension, formed in the burden of the numerical models, confirmed that the burden was not significantly fractured. Therefore, complete damage of the burden could not develop in Tests 1 and 2 (in the field tests and in the numerical models).

- The numerical analysis of Tests 4 and 5 also provided answer to the behaviour of the rock mass in these field tests. It was observed that, the generated fractures in the burden combined with the natural joint condition of the burden, increased the possibility for blocks to rotate and move within the burden. The rock blocks in the vicinity of the wall were ejected upon the arrival of stress wave. The remaining portion of the heavily fractured rock blocks in the burden were ejected by the gas expansion.
- The numerical analysis of the rock support mimicked the rock support response. More conservative elongation and deflection of the support system was observed in the models. It can be concluded that the presented approach can already be a tool to be used to simulate the behaviour of other rock support systems. However, the behaviour of other rockbolts, has to be investigated separately before the new bolts are used in the model.

ACKNOWLEDGEMENTS. The tests were conducted within the frame of two research projects supported by Vinnova (Sweden's innovation agency), EU 7th framework, LKAB and Boliden AB, and Centre of Applied Mining and Metallurgy (CAMM) at LTU. This work was financially supported by LKAB, Boliden, Centre of Advanced Mining & Metallurgy at LTU (CAMM/CAMM2) and the I2Mine project which are gratefully acknowledged. The LKAB Mining Company in Kiruna is gratefully acknowledged for providing the opportunity to conduct the tests at this mine.

References

[1] Ortlepp, W. (1969). An empirical determination of the effectiveness of rockbolt support under impulse loading. In: Brekke TL, Jorstad FA (eds) Proceedings of the international symposium on large permanent underground openings, Universitats - forlaget, Oslo, Norway, pp. 197-205.

[2] Ortlepp, W. (1992). The design of support for the containment of rockburst damage in tunnels–an engineering approach. In: Proc. int. symp. on rock support in mining and underground construction, pp. 593-609.

[3] Tannant, D.D., McDowell, G.M. and McCreath, D.R. (1994). Shotcrete performance during simulated rockbursts. In: Workshop on applied rockburst research (eds) IVth south american congress on rock mechanics, (SOCHIGE), Santiago, pp. 241-248.

[4] Tannant, D.D., Brummer, R.K. and Yi, X. (1995). Rockbolt behaviour under dynamic loading: field tests and modelling. International Journal of Rock Mechanics and Mining Sciences & Geomechanics Abstracts 32(6):537-550.

[5] Hagan, T.O., Milev, A.M., Spottiswoode, S.M., Hildyard, M.W., Grodner, M., Rorke, A.J., Finnie, G.J., Reddy, N., Haile, A.T. and Le Bron, K.B. (2001). Simulated rockburst experiment-an overview. Journal of the Southern African Institute of Mining and Metallurgy 101(5):217-222.

[6] Espley, S.J., Heilig, J. and Moreau, L.H. (2002). Assessment of the dynamic capacity of liners for application in highly-stressed mining environments at INCO Limited. In: Potvin Y, Stacey TR, Hadjigeorgiou J (eds) Proceedings of the international seminar on surface support liners, Johannesburg, South Africa, July 2002 pp. 187-192.

[7] Archibald, J.F.,Baidoe, J.P. and Katsabanis, P.T. (2003). Rockburst damage mitigation benefits deriving from use of spray-on rock lining. In: Potvin Y, Stacey TR, Hadjigeorgiou J (eds) Proceeding of third international seminar on surface support liners: Thin spray-on liners, shotcrete and mesh, Universite´ Laval, Quebec City, Canada, August 2003 Section 19 pp. 169-178.

[8] Ansell, A. (1999). Dynamically loaded rock reinforcement. PhD Thesis, Institutionen för byggkonstruktion - KTH Universitet.

[9] Ansell, A. (2004). In situ testing of young shotcrete subjected to vibrations from blasting. Tunn Undergr Sp Technol 19(6):587-596.

[10] Andrieux, P.P., Turichshev, A., O´Connor, C.P. and Brummer, R.K. (2005). Dynamic Testing With Explosive Charges of Rockburst-Resistant Ground Support Systems at the Fraser Nickel Mine. Report to Falconbridge Limited Mine Technical Services, Final Version, September 2005 Itasca Consulting Company Inc. Sudbury, Canada.

[11] Heal, D., Hudyma, M., Langille, C., Potvin, Y., Butcher, R., Ball, R. and Hartmann, B. (2005). In-situ testing of ground support performance under strong dynamic loading. In: Potvin Y, Hudyma M (eds) Proceedings of the 6th international symposium on rockbursts and seismicity in mines, Australian Centre for Geomechanics, Perth, Australia, pp. 85-94.

[12] Heal, D. and Potvin, Y. (2007). In-situ Dynamic Testing of Ground Support Using Simulated Rockburst. In: Potvin Y (eds) Proceeding of fourth international seminar on 'deep and high stress mining', Australian Centre for Geomechanics, Perth, Australia, pp. 373-394.
[13] Heal, D. (2010). Observations and analysis of incidences of rockburst damage in underground mines. Doctor of Philosophy of Civil and Resource Engineering, School of Civil and Resource Engineering, University of Western Australia.
[14] Shirzadegan, S., Nordlund, E. and Zhang, P. (2016a). Large scale dynamic testing of rock support system at Kiirunavaara underground mine. Rock Mechanics and Rock Engineering 49(7):2773-2794.
[15] Shirzadegan, S., Nordlund, E. and Zhang. P. (2016b). Large scale dynamic testing of rock support at Kiirunavaara – Improved test design. Tunneling and Underground Space Technology 59:183-198.
[16] Chen, S.G. and Zhao, J. (1998). A study of UDEC modelling for blast wave propagation in jointed rock masses. International Journal of Rock Mechanics and Mining Sciences 35(1):93-99.
[17] Chen, S.G., Zhao, J. and Zhou, Y.X. (2000). UDEC modeling of a field explosion test. International Journal for Blasting and Fragmentation 4(2):149-163.
[18] Wang, Z.L., Konietzky, H. and Shen, R.F. (2009). Coupled finite element and discrete element method for underground blast in faulted rock masses. Soil Dynamics and Earthquake Engineering 29(6):939-945.
[19] Zhang, P., Yi, C.P., Nordlund, E., Shirzadegan, S., Nyberg, U., Malmgren, L. and Nordqvist, A. (2013) Numerical back analysis of simulated rockburst field tests by using coupled numerical technique. In: Potvin Y (eds) Proceeding of seventh international symposium on ground support in mining and underground construction, Australian centre for Geomechanics, Perth, pp. 565-585.
[20] Deng, X.F., Chen, S.G., Zhu, J.B., Zhou, Y.X., Zhao, Z.Y. and Zhao, J. (2015). UDEC–AUTODYN hybrid modeling of a large-scale underground explosion test. Rock Mechanics and Rock Engineering 48(2):737-747.
[21] Andersson, U.B. (2010). Geology and Structures for Level Z741 Blocks 9 and 12. Internal Report LKAB Kiruna, Sweden.
[22] Andersson, U.B. (2011). Tättkartering runt skjutskador ort 93 oh 95 Z741. Internal Report LKAB Kiruna, Sweden.
[23] Hallquist, J.O. (2006). LS-DYNA theory manual. Livermore, California.
[24] Riedel, W., Thoma, K., Hiermaier, S. and Schmolinske, E. (1999). Penetration of reinforced concrete by BETA-B-500 numerical analysis using a new macroscopic concrete model for hydrocodes. In: Proceedings of the 9th international symposium on the effects of munitions with structures, Berlin-Strasburg.
[25] Borrvall, T. and Riedel, W. (2011). The RHT concrete model in LS-DYNA. In: Proceedings of the 8th european LS-DYNA users conference, Strasbourg.

[26] Kuhlemeyer, R.L. and Lysmer, J. (1973). Finite element method accuracy for wave propagation problems. Journal of Soil Mechanics & Foundations Div 99(Tech Rpt).
[27] Malmgren, L. and Sjöberg, J. (2006). Bergmekaniska analyser för ny huvudnivå i KUJ (1365). Utredning nr 06-797 LKAB Sweden.
[28] Malmgren, L. and Nordlund, E. (2008). Interaction of shotcrete with rock and rock bolts—A numerical study. International Journal of Rock Mechanics and Mining Sciences 45(4):538-553.
[29] Malmgren, L. (2008). Design basis - Kiirunavaara mine. Internal report LKAB Kiirunavaara LKAB mine.
[30] Brandshaug, T. (2009). An Initial Evaluation of the Effects of Seismic Motion on a Footwall Drift at LKAB's Kiirunavaara Mine. GT09-4001-1 LKAB Kiirunavaara mine.
[31] Malmgren, L. and Nordlund, E. (2006). Behavior of shotcrete supported rock wedges subjected to blast-induced vibrations. International Journal of Rock Mechanics and Mining Sciences 43(4):593-615.
[32] Malmgren, L. (2007). Strength, ductility and stiffness of fibre-reinforced shotcrete. Magazine of Concrete Research 59(4):287-296.
[33] Saiang, D., Malmgren, L. and Nordlund, E. (2005). Laboratory tests on shotcrete-rock joints in direct shear, tension and compression. Rock Mechanics and Rock Engineering 38(4):275-297.
[34] Shirzadegan, S. (2020). Development of a Methodology for Dynamic Testing of Rock Support – Field tests and numerical analysis. PhD, Luleå University of Technoogy.
[35] Itasca Consulting Group I (2015). UDEC-Universal Distinct Element Code, Version 6.0, User Manual, Minnesota, USA.
[36] Voyzelle, B., Anderson, T., Quesnel, S., Eagleson, R. and Trottier, J. (2014). Laboratory Testing of Static and Dynamic Behaviours of Atlas Copco MN24 Swellex Bolts. Canmet mining project P-001335.001.
[37] Thyni, F. (2014). Design of Shotcrete for Dynamic Rock Support by Static Testing. Master Thesis, Luleå University of Technology.